Advanced Composites and Hybrid Materials (2025) 8:65
https://doi.org/10.1007/s42114-024-01107-x

RESEARCH

Expectations vs. reality in nacre-like composites: dominating role of particle packing and polymer confinement in mechanical performance

V. Semeykina[1] · C. Appiah[1] · S. Rothberg[1] · S. Heinrich[1] · D. Giuntini[1,2] · G. A. Schneider[1]

Received: 10 July 2024 / Revised: 5 November 2024 / Accepted: 27 November 2024

Abstract
After decades of research, mimicking the intricate structure of nacre shells with flawlessly packed blocks remains a laborious task in composite material design. For practical reasons, less ideal alternatives with reduced packing densities below 70 vol.% are often being explored. However, the extent to which the features of the nacre structure can be exploited remains unclear. This paper investigates whether mimicking nacre design in non-densely packed composites can still deliver exceptional mechanical performance. A wide range of ceramic particles (80–100 µm, including spheres and platelets) and methacrylate-based polymers was studied. All the composites exhibited little variation in strength (100–150 MPa) and E-modulus regardless of hierarchical structure, particle size, shape, or interfacial bonding, highlighting the greater importance of particle packing over these factors for ceramic loadings below 65 vol.%. In particular, the benefits of micron-sized anisotropic particles were diminished by the fundamental challenges in aligning such blocks: although these assemblies significantly enhanced fracture resistance, the elastic modulus was still lower than expected (25 GPa). A polydisperse mixture of irregularly shaped micron-sized particles surprisingly achieved a high elastic modulus of 20 GPa, suggesting that an optimized size distribution can provide benefits comparable to those of particle anisotropy. Composites loaded with small particles (< 500 nm) exhibited two key effects: the solvation shells contributed to the total organic content significantly, limiting the maximum ceramic loading, and the polymer confined within small interparticle voids exhibited increased stiffness, leading to more brittle fracture despite the abundance of organic phase. Both phenomena should be accounted for in theoretical simulations and the practical design of composite materials.

Keywords Nacre material · Bio-inspired composite · Nanoresin · Self-assembly · Mechanical properties · Polymer confinement

1 Introduction

Technological progress creates demand for new materials with superior mechanical properties, which requires intricate material designs. Composite materials can combine reasonable strength with good stiffness and hardness as well as damage tolerance due to their ability to delocalize and dissipate stresses between their constituting elements. The high strength of ceramics and the improved stress dissipation by polymers are often combined to create composites with excellent performance. Ceramic-polymer composites have found use in a wide range of applications from industrial construction materials [1] reinforced with various fibers and fillers to sophisticated dental materials [2–4] that evolved from simple metallic amalgams to complex engineered ceramics and composites such as nanoresins (ceramic-in-polymer) and polymer-infiltrated ceramic networks.

The bio-inspired nacre-like tough composites have been a popular topic in material science over the past 30 years [5]. A thorough investigation of toughening mechanisms in natural materials helped to identify the key to the mystery of their exceptional mechanical performance: a complex hierarchical structure enabling effective stress distribution from macro- to nanoscale [5, 6]. To ensure high toughness, the structure must inherently contain at

✉ V. Semeykina
viktoriyacatalysis@gmail.com

1 Hamburg University of Technology, Hamburg, Germany

2 Eindhoven University of Technology, Eindhoven, Netherlands

Published online: 20 December 2024

least two elements — "bricks" of the hard phase for high stiffness and strength and a softer "mortar" phase for effective stress distribution leading to toughening and damage tolerance. Many materials like nacre-mimetic composites [1, 7–9], fiber-reinforced composites [10, 11], and bio-inspired coatings [12] exhibit multiple repetitive levels of brick-and-mortar structures to distribute the initial macroscopic stresses to the lower hierarchical levels, i.e., microscopic plastic or viscoelastic bond deformations or crack meandering through nano-interfaces. High structural anisotropy [13] also plays an important role in toughening, with a minimal aspect ratio of the bricks required to maximize mechanical performance.

As thoroughly as nacre has been studied, the practical replication of its structure remains a major challenge. One of the main limiting factors is achieving a very dense packing of the bricks [14, 15]. Such packing results in both high stiffness and strength by minimizing the volume between the bricks filled with the softer phase or air. In nature, these orderly structures are being built step-by-step over weeks using biological nano-machinery [16–18], while in the lab, the researchers have to resort to costly top-down approaches [19] and self-assembly principles [20, 21]. The latter got special attention as a promising scalable method, where the assembly of the particles is governed by the competition between enthalpy and entropy gains and may be supported by external forces (magnetic [22], gravitation, centrifugation, capillary, surface pressure). The quality of packing is however limited by the number of defects always occurring in this stochastic process [23], which accumulate as the system is scaled up.

To maintain the quality of particle packing at an acceptable level, researchers often have to limit the size of the assembled system to a micro-scale, at least in one dimension. This constraint led to a large number of promising proof-of-concept studies on microbars and thin films [24, 25] but limited the preparation of the larger bulk samples [26, 27]. The latter involves the particle assembly in thin micrometer-sized films with subsequent stacking of the sheets [8] or assembly in sub-micron voids created by the freeze-casting [28] method with subsequent freeze-drying and structure densification. The best examples of such nacre-like composites are reported to have mechanical strength of up to 300 MPa, elastic moduli of up to 30–50 GPa, and fracture toughness K_{IC} of up to 5–30 MPa$\cdot\sqrt{m}$ [29–34]. The composites featuring polymer-infiltrated ceramic scaffolds typically show higher stiffness and more brittle behavior, while the materials produced by the assembly of bricks in a softer matrix usually have a more plastic response and better tolerance to defects. The best mechanical performance is usually achieved by using dilute suspensions [8] to ensure an improved packing of particles, which can potentially limit the preparation of such nacre-inspired materials in practice, especially for applications demanding large quantities of material.

This paper aims to investigate whether mimicking nacre design in non-densely packed bio-inspired composites produced from more concentrated colloids (up to 50 vol.%) can still deliver improved mechanical performance in terms of E-modulus, strength, and toughness. We prepared a series of ceramic-in-polymer composites with various ceramic blocks and 25–75 vol.% of the polymer phase. It was found that the hierarchical structure, size, and shape of the ceramic fillers (monodisperse spheres with a diameter from 80 to 450 nm, polydisperse 1–10 µm particles with an irregular shape, 0.15×10 µm and 1×100 µm platelets) exhibited little effect on the mechanical strength and E-modulus when the packing was not *exceptionally* tight (50–65 vol.%), which is typically the case for many reported self-assembled nacre-inspired bulk composites. Using a polydisperse mixture was found to provide strength and stiffness comparable to those for composites with anisotropic building blocks but with fewer challenges related to the alignment of high-aspect-ratio particles. Interesting effects were observed for composites loaded with small particles (< 500 nm): the solvation shells significantly contributed to the total organic content, limiting the maximum ceramic loading, and the polymer confined within small interparticle voids exhibited increased stiffness, leading to more brittle fracture despite the abundance of organic phase. Both phenomena should be accounted for in theoretical simulations and the practical design of composite materials.

2 Experimental section

2.1 Production of macroscopic composites

The information about the used chemicals, the synthesis, and surface modification of the ceramic building blocks can be found in the Supporting Information (See SI Experimental section). The preparation of composite materials was as follows.

Typically, 0.5–1.0 g of a ceramic phase was thoroughly sonicated with 1–2 ml of a monomer solution at 100 Hz in 0.5–1.0-s pulses for 5–30 min using a UP100H Hielsher Ultrasound Technology sonicator (140-µm amplitude and 125 W cm^{-2} acoustic power). Once the mixture was homogenized, the colloid was mixed with 0.5–5 wt% of the DCP initiator and centrifuged at 1000–18,500 × g for 5–60 min depending on the particle density and size to produce dense composite pellets. The pellets were transferred in the sealed tubes to an oil bath and left to radically polymerize at 80–105 °C for 15–18 h. Alternatively, a centrifuged pellet or a highly concentrated ceramic-in-polymer paste was pressed in a hot-pressing die under up to 60–100 MPa to remove the

excess of the liquid monomer. By regulating the liquid content in the paste and the rate of pressure buildup (5–60 MPa/min), it was possible to control to some degree the amount of monomer squeezed out during the pressing step resulting in composites with various ceramic content. The pressed pellets were quickly pre-polymerized in a hot press for 30–60 min at 60–100 ^{0}C to ensure easy pellet removal and then fully cured in a sealed vessel in an oven at 120 °C for 16 h. The final cured composites were cut into ~ 1 × 1 × 10-mm bars and heat treated again at 120 ^{0}C in an oven in the air for 16 h to remove potential traces of water absorbed by some polymer mixtures during the cutting in the aqueous environment (Fig. 1).

2.2 Characterization methods

The size and zeta potential of the nanoparticles in aqueous dispersions were determined by dynamic light scattering (DLS) using a Zetasizer Nano Series instrument (Malvern). The content of the organic phase in the composites was estimated by thermogravimetric analysis (TGA) with a METTLER TOLEDO TGA/DSC 1. The probe was held in N_2 flow at 125 °C for 30 min to remove adsorbed water molecules and heated up to 800 °C in air at the rate of 3 K/min. The weight loss was calculated for the temperature range of 125–800 °C. An optical Olympus microscope, an SNE-3200M Tabletop SEM (5kV acceleration voltage), and Zeiss Supra VP55 SEM were used to analyze the microstructure of the composites. Particle sizes were estimated from the images using ImageJ on a set of 50–70 data points.

Flexural stress–strain curves were obtained by three-point bending tests using an in-house bending setup [35], loading the samples at a constant displacement rate of 0.5 µm/s. The flexural stress σ_f and strain ε_f were calculated on the average of three measurements using the following equations:

$$\sigma_f = \frac{3FS}{2wh^2}\varepsilon_f = \frac{6Dh}{S^2},$$

where F is load in N, S is lower support span in mm, w and h is sample's width and height in mm, and D is absolute displacement in mm. The lower support span to sample height ratio S/h was chosen to be 8–11 to reduce the contribution of shear components to the apparent flexural modulus (see more in SI, "On the challenges of mechanical characterization," Fig. SI1). To evaluate fracture behavior, the bars were pre-notched with a 300-µm crack and loaded in a mode with partial unloading during the crack growth, in which the displacement was reduced by ~ 5 µm after a registered drop in the load. The complications of the optical crack monitoring made the calculation of the fracture toughness parameter for all studied samples challenging. Composite toughness in J/m^2 was calculated by dividing the area under the load–displacement curve (accounting for the unloading segment) by the cross-section area generated by the resulting crack. Nanohardness of the composites was tested using a Nanoindenter iMicro (KLA/SchäferTec) with a 300-µm Berkovich tip, using the advanced dynamic E and H measurement method, with a constant strain target of 0.2

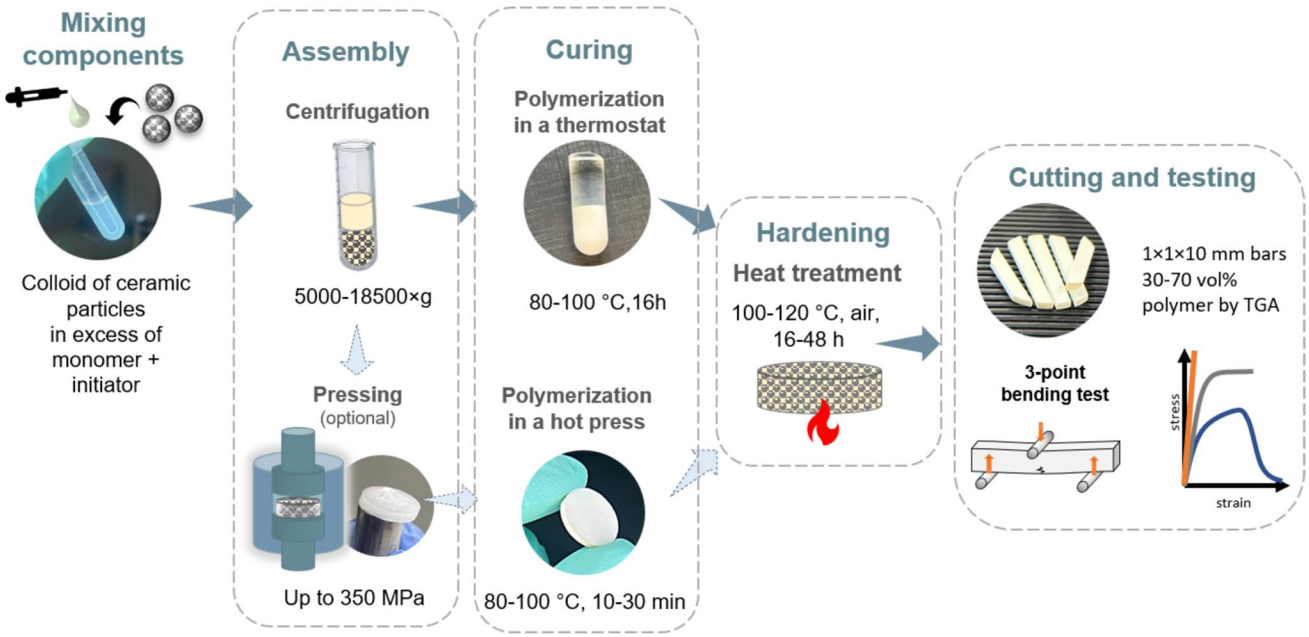

Fig. 1 A typical scheme for the preparation of bulk composite materials in this study

s^{-1}, a dynamic displacement target of 2 nm, and a target oscillation frequency of 110 Hz. The samples were loaded up to a 5000-nm depth.

3 Results

3.1 Characterization of the composites' constituents

The composites were prepared using a wide range of nanoparticles as a ceramic phase: 80–450-nm monodisperse silica spheres, ~ 0.15 × 10 µm alumina platelets, ~ 1 × 75 µm silica platelets, irregularly shaped polydisperse 1–10-µm alumina particles with distribution maximums between 2 and 5 µm, and ~ 7-µm supraballs of silica spheres (Table 1; Fig. 2). To improve dispersion and bonding with the polymer matrix, the nanoparticle surfaces were modified with aminopropyl-, methylmethacrylate-bearing organic silanes or vitrimers. TGA estimations showed that both silanes and vitrimers formed multiple surface layers, adding 2–5 wt% of organic material to the nanoparticles. MMA-propyl-modified particles were expected to form permanent covalent bonds with the polymer, while aminopropyl coatings would enable weaker, interchangeable "self-healing" hydrogen bonds. Vitrimer coatings provided an intermediate link

Table 1 Characteristics of the different particles used for the preparation of composites

Ceramic particles	Size by SEM	Size distribution by DLS	Aspect ratio	Surface groups	TGA weight loss, wt%
Silica spheres	80 ± 20 nm 200 ± 25 nm 320 ± 35 nm 450 ± 50 nm	80 ± 20 nm 200 ± 30 nm 320 ± 30 nm 450 ± 50 nm	1	Silanols MMA-propyl-, aminopropyl-	2.5–5.0wt%
Alumina particles with irregular shape	4 ± 2 µm	4 ± 3 µm	~ 1–2	MMA-propyl-	1.3
Alumina platelets	(0.15 ± 0.05) × (10 ± 3) µm	8 ± 5 µm	67	MMA-propyl-, aminopropyl-, vitrimer-	2.0 2.1 3.1
Silica platelets	(1.0 ± 0.3) × (75 ± 30) µm	80 ± 15 µm	75	Silanols, MMA-propyl-	1.3
Silica supraballs	7 ± 3 µm	–	1	1500 Da PHEMA coating, 1500 Da PEO-PPG-PEO coating	11.0 10.5

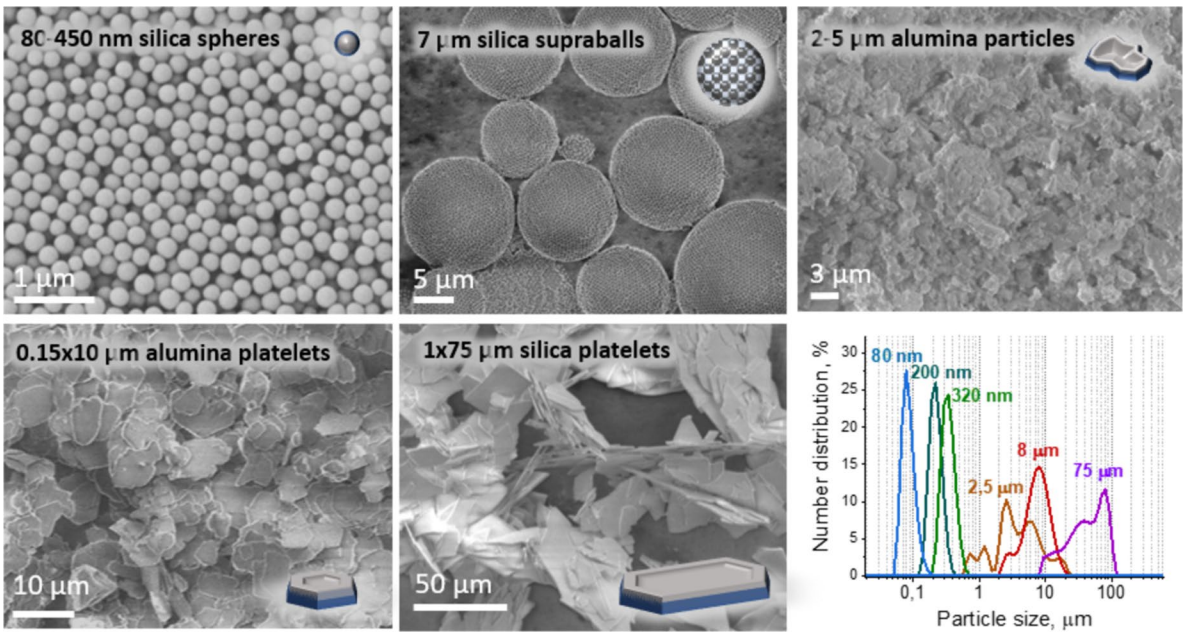

Fig. 2 Size and shape characterization of the ceramic blocks in composites by SEM and DLS

with both H-bonding and covalent connections between the condensable groups.

The soft phase was primarily polymerized using methacrylate-based monomers (MMAs) with various functionalities. A more rigid response was achieved with monomers forming permanent covalent bonds through cross-linking (DVB, EGDMA, TEGDMA; see Fig. SI2 a,b) or side-group condensation reactions (GMA and HEMA). In contrast, pure PMMA or PHEMA exhibited more plastic behavior due to weaker, exchangeable Van der Waals and, in the latter case, hydrogen bonds, similar to those found in biopolymers in nacre shells, which are important for composite performance. Hydrogen bonds (0.1–0.4 eV) are expected to be stronger than Van der Waals interactions (~0.1 eV) but still weak enough to impart plasticity and self-healing properties upon fracture. The effect of polymerization kinetics on mechanical performance was investigated by varying the initiator content. An initiator concentration of 1–2 wt% (Mw ~ 10–14 kD) produced composites with optimal mechanical properties (Fig. SI2 c,d).

The integrity of the final bulk material was found to be very sensitive to the curing conditions. Pre-existing cracks and heterogeneities might complicate the screening process since they dominate the mechanical response and provide little information about the true mechanical properties of an underlying structure. Proper homogenization and minimizing volume shrinkage were critical throughout the preparation process, achieved by reducing solvent or monomer evaporation and avoiding too slow or too high polymerization rates. For more details on common practical challenges, refer to the Supporting Information chapter "The typical challenges in the preparation of ceramic-in-polymer composites — shrinking, crack formation, porosity, inhomogeneity".

3.2 Screening of polymer composition and content

Polymer composition significantly influenced the composites' mechanical behavior (Fig. 3 a). MMA- and HEMA-based samples exhibited the best mechanical properties, while pure GMA, styrene, and cross-linked mixtures showed lower strength and flexural modulus. The reduced E-modulus and earlier crack onset in GMA-, TEGDMA-, and DVB-containing samples likely resulted from microcracks formed during preparation due to the insufficient plasticity of the polymer framework. Maintaining adequate plasticity through hydrogen bonds in PHEMA or van der Waals bonds in PMMA helps prevent microcrack formation during polymerization/heat treatment and improves stress distribution under load. In addition, the higher evaporation enthalpy of polar HEMA reduced premature monomer evaporation during polymerization, thereby decreasing porosity in the final composite (see the SI Section "Practical challenges in the preparation of ceramic-in-polymer composites …").

Similar to many reported bio-inspired composites, the ceramic content in the studied samples ranged from 30 to 70

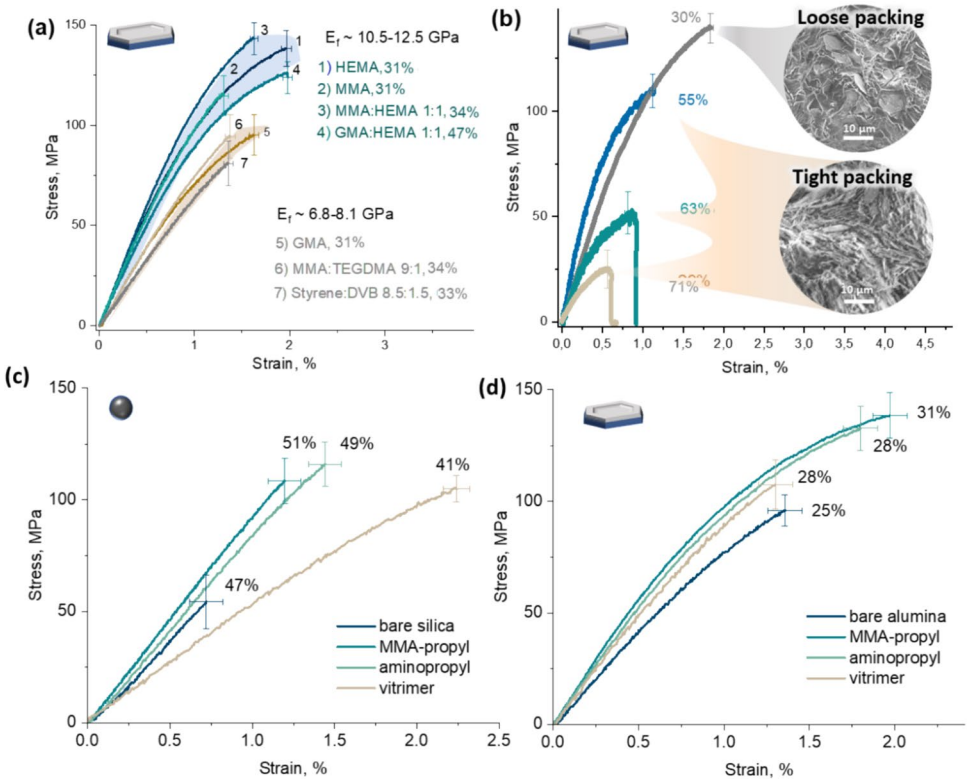

Fig. 3 Representative stress–strain curves in a three-point bending test for the composites with **a** MMA-modified alumina platelets having various polymer compositions; **b** vitrimer-modified alumina platelets having various PHEMA polymer contents; **c** 280-nm silica spheres with various surface treatments in PHEMA/PMMA = 1:1 mixture; and **b** 0.15 × 1.0 µm alumina platelets with various surface treatments in PHEMA. The "loosely packed" composites were produced by centrifugation; the "tightly packed" ones were additionally uniaxially pressed at 65 MPa with various loading rates. The volume fraction of the ceramic, estimated by TGA, is given on the graph in vol. % for each sample

vol.% (TGA estimate), much higher than the ~ 90–95 vol.% of the mineral matrix in densely packed nacre structures [36] (Fig. 3 b). Samples with 30–55 vol.% ceramic content (45–70% polymer) demonstrated consistent mechanical response, flexural strengths of 100–150 MPa, flexural moduli of 8–15 GPa, and improved ductility for larger ceramic blocks. Nanohardness at 1–5-µm indentation depths ranged from 0.5 to 1.2 GPa with the nanoindentation-based elastic modulus of 10–25 GPa, typical for ceramic-in-polymer dental composites [11, 37] (Fig. SI3). These properties indicate that the polymer phase plays a key role in compression and bending. The highest stiffness achieved was 25 ± 1 GPa, with 45 vol.% polymer filling all voids between platelets. Based on this data, the densest achieved packing density of platelets in these samples is estimated to be ~ 55 vol.%.

Samples with lower polymer content (20–45 vol.%, TGA) exhibited poorer mechanical properties and were more prone to crumbling and delamination. In the composites with insufficient nanoparticle packing, the reduced polymer content increased porosity and weakened binding between ceramic blocks. To eliminate the influence of porosity on mechanical performance, the polymer-deficient composites were excluded from the analysis of structure-related parameters affecting mechanical properties.

3.3 Screening of particle surface modification

The impact of surface treatment with different functional groups on mechanical response was difficult to interpret (Fig. 3c,d). For instance, while MMA-propyl and aminopropyl-modified surfaces were anticipated to have significantly different interactions with the polymer phase (strong covalent vs. weak H-bonding), the differences in their corresponding stress–strain curves were minimal for both spherical and platelet fillers. It was also found that different surface groups influenced the solubilization behavior of particles in the monomer, especially the smaller ones < 500 nm, sometimes facilitating aggregation and resulting in lower ceramic loading, particularly with bare and vitrimer-modified fillers. Consequently, the effects of altered polymer-surface interactions and changes in ceramic loading are difficult to separate. However, the change in ceramic loading appears to have a greater impact on mechanical behavior than the alteration of surface chemistry itself, which will be discussed in more detail in the Section 4.

3.4 Screening of the size and shape of the ceramic blocks

None of the studied composites achieved the theoretically possible maximum packing of ceramic building blocks, estimated as ~ 75 vol.% for spheres and ~ 90 vol.% for platelets, which are typical in both commercial applications [11] and research papers [22, 38]. To attain the densest practically achievable packing, ceramic building blocks were centrifuged at high acceleration speeds (1000–18,000 × g, depending on particle size). To further densify the structure, the wet, unpolymerized composites were pressed at 65 MPa, increasing the ceramic volume fraction to > 55 vol.%. Therefore, the effects of particle size and shape were examined in the composites with a packing density of ~ 35–65 vol.%.

Surprisingly, despite a three-order magnitude variation in particle sizes and a one-order magnitude variation in aspect ratio, the differences in stress–strain curves were not as pronounced as expected (Fig. 4a; also see Sect. 4). Whether large or small, spherical or elongated, all studied ceramic blocks had a limited effect on initial linear elastic stiffness (E ~ 10–25 GPa), albeit a more pronounced effect on ductility at high strains. For comparison, the E-modulus of nacre is supposed to reach 70–110 GPa with the densest platelet packing [39].

A similar trend was observed in the hierarchical composites made from ~ 7-µm supraballs composed of polymer-glued small silica spheres: the mechanical response remained largely unchanged despite an added level of complexity, consistent with previous findings on polymer-rich compositions (Fig. 4 b; Fig. SI4). Given the high polymer content in these samples, differences in ductility likely stem from the activation of plastic deformation in the second polymer within the supraballs, rather than anticipated crack deflection within the hierarchical structure. The PHEMA polymer, with its network of hydrogen bonds, resulted in a stiffer response, while a block copolymer with weaker Van der Waals bonds between the chains led to more ductile behavior at higher strains.

4 Discussion

Many studies on bioinspired composite materials emphasize the sophisticated design at the nano-, micro-, and macroscale as essential for improving mechanical properties, a hypothesis that without doubt holds true from a fundamental perspective. However, the situation becomes more complex technically, as densely packed nacre-like composites are challenging to produce, especially using feasible industrial methods. Our findings suggest that factors beyond tailored anisotropy and hierarchy — such as total ceramic loading and the absolute size of the soft phase domains — influence the mechanical response of upscaled ‘non-ideal’ nacre-inspired composites to a greater extent. Technologically, this implies that optimizing the particle size distribution of the ceramic filler can already improve mechanical properties (in particular, stiffness) without extensive efforts in the laborious self-assembly of ordered structures. Moreover, the composite’s capacity for plastic

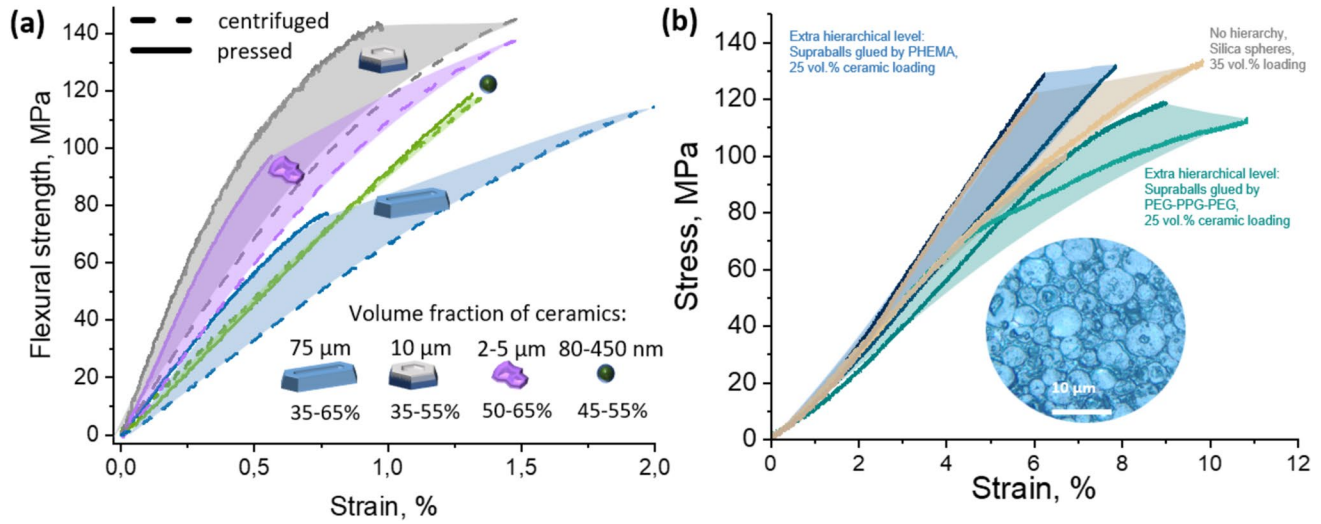

Fig. 4 Stress–strain curves for the best-performing composites produced with various ceramic blocks: **a** various types of MMA-modified ceramic platelets, irregularly shaped particles, and spheres; **b** composites with an additional hierarchical level consisting of spray-dried supraballs of MMA-modified silica spheres glued with 10 vol.% of PHEMA or block-copolymer. Note that the E-modulus in the second graph does not represent the true composite stiffness since the bars were loaded under non-standard conditions

deformation can be influenced by the polymer's state in confinement, which correlates with the size of the polymer-filled intraparticle voids and, ultimately, the absolute particle size. This phenomenon should be considered in the design of ceramic-in-polymer composites, as materials with ceramic particles below a certain size threshold may exhibit more brittle behavior than anticipated.

4.1 Composite mechanical properties vs. organic content and particle aspect ratio

Interpretation of the observed mechanical behavior The screening of the ceramic phase across a wide range of particle sizes and aspect ratios highlighted the critical role of organic content in the mechanical response (Fig. 5 a).

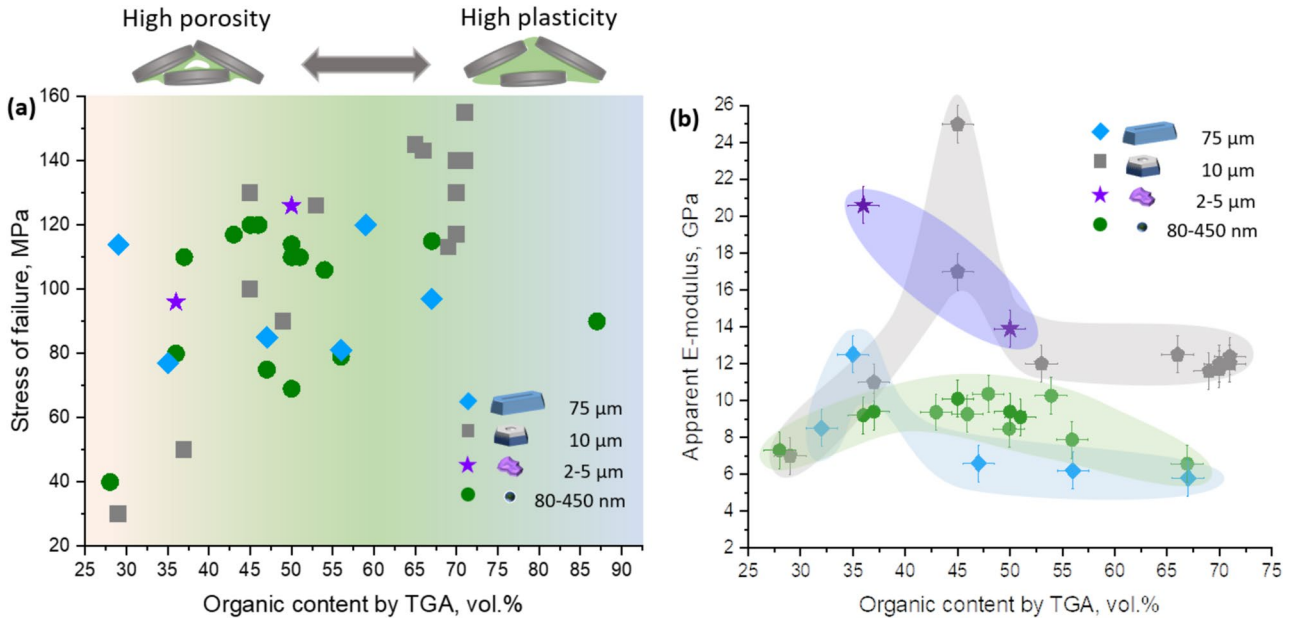

Fig. 5 **a** Failure stress and **b** apparent flexural modulus in a three-point bending test for the composites with various polymer volume fractions. Polymer-rich samples were densified by centrifuging at 1000–18000 × g; polymer-deficient samples were additionally densified by pressing the precipitate at 65 MPa. Polymer phase—PHEMA and PHEMA-containing mixtures

Polymer-rich composites, as expected, exhibited plastic behavior with the highest failure stress, while reducing polymer content in the intraparticle voids led to the formation of (micro)pores in loosely packed ceramic assemblies. These polymer-deficient samples showed significantly lower mechanical strength (< 50 MPa) with high dispersion (~ 50–100%) and a reduced elastic modulus (4–7 GPa) with less data variation (~ 20–30%), suggesting that the E-modulus is a more reliable parameter for screening materials with suspected residual porosity. By adjusting particle packing density and polymer content through centrifugation and pressing, we identified optimal conditions where interparticle voids were minimized and fully filled with polymer (between 40 and 50 vol.% of organic by TGA), resulting in the highest E-modulus for non-ideal particle packing (Fig. 5 b). The porosity of the best-performing samples was estimated to be 2–8% depending on the filler based on the pycnometry measurements (Table SI1).

The elastic modulus of composites is expected to increase with particle content, though this relationship is non-linear and heavily influenced by particle size and shape [40–43]. Theoretical models predict that high-aspect-ratio particles significantly increase the effective modulus (anisotropically) if they are well-aligned [44]. Conversely, larger particles are expected to yield a slightly lower modulus due to their smaller specific surface area, which reduces the energy required for debonding from the polymer matrix [45]. The experimental data showed the following trend in the maximal achieved composite elastic moduli: E(80–450 nm spheres) ≤ E(75 µm platelets) < E(2–5 µm irregular particles) ≤ E(10 µm platelets) (Fig. 5 b). Polydisperse irregularly shaped particles and platelets generally increased the stiffness at similar organic phase content, indicating that the positive effect of high-aspect ratios outweighed the negative impact of particle size on the E-modulus. However, there was no straightforward correlation between nanoparticle aspect ratio and modulus, suggesting that factors like imperfect particle alignment and excess soft phase may play a more decisive role than previously assumed [46, 47].

These results bring us to the problem of insufficient particle packing density in the studied composites. Assuming that the maximum packing density corresponds to the highest elastic modulus for the same type of filler and polymer, we evaluated the minimal amount of the polymer needed to fill up all the voids (see Figs. 4 b and 5 b). Based on the approximate positions of the maximums in Fig. 5 b, the best-achieved particle packing density of composites with 80–450-nm spheres is 45–55 vol.%; 2–5-µm irregularly shaped particles — between 50 and 65 vol.%; 10 µm platelets — around 55 vol.%; and 75-µm platelets — 55–65 vol.%. These densities are much lower than the theoretical value of > 95 vol.% for platelets but approach the 74 vol.% limit for the densest packing of monodisperse spheres. Moreover, for colloidal spheres with an ~ 5-nm "monomer solvate + surface ligand" shell, the maximum theoretical ceramic fraction drops to 55–65 vol.% for 100–300-nm spheres (see SI "Theoretical Estimation of Organic Volume Fraction," Fig. SI5). These calculations along with SEM observations (Fig. SI6) suggest that small spherical particles in the studied composites are already packed to the physical limit, meaning that the stiffness of such composites cannot be further improved solely by a higher particle loading. In contrast, similar estimations for large platelets result in a theoretically densest ceramic loading of ~ 88 vol.%, indicating significant potential for improvement.

Possible approaches to improve the mechanical performance These findings lead to the following questions: which phenomena decrease the packing density of nanoparticles and what can be done to avoid them? We will discuss the following key factors influencing particle packing density — colloidal stabilization of particles in suspensions, the role of the aspect ratio, and particle size distribution.

Colloidal stability in self-assembly Colloidal stabilization of particles in suspensions depends on the nature of particle surface groups and is well described by the DLVO theory on colloidal interactions [48]. According to this model, systems with predominantly attractive interactions between particles tend to form aggregates upon nanoparticle collision, leading to loosely packed structures. Stabilized systems with primarily repulsive interactions, on the other hand, allow reversible aggregation/dispersion of particles, eventually resulting in a more thermodynamically favorable configuration with denser particle packing. A similar trend is observed during the pressing of centrifuged wet "green bodies": in systems with non-attractive interactions, particles can freely move and achieve denser packing, while attractive interactions hinder reorganization within the ensemble.

In practical terms, colloid stability depends on two key factors: (1) the thickness and density of the stabilizing shell on the particle surface, which ensures that particles bounce upon collision, and (2) the frequency of particle collisions, i.e., concentration. Creating an effective stabilizing shell in aprotic organic media is challenging, as charge repulsion cannot be fully utilized, leaving steric stabilization as the primary option. The absence of attractive H-bonding between the particles in a low-polarity monomer typically led to a denser colloidal crystal — 49% ceramic loading for MMA-silica in the HEMA/MMA 1:1 mixture vs. 32% ceramic loading for aminopropyl-silica in HEMA (Fig. SI6). The differences in colloidal stabilization can be reduced by adjusting the monomer composition — 51% vs. 49% ceramic loading for both silane modifications in the HEMA/MMA 1:1 mixture (Fig. 3 d). Both insufficient and excessive (multilayer) group coverage also impacted stabilization efficiency:

MMA-propyl-modified silica colloids with different coverage (2.5, 3.0, and 4.9 wt% by TGA) yielded varying degrees of structural order, with the thinnest silane layer producing the most ordered colloidal crystal (Fig. SI6). Nonetheless, the packing order had minimal impact on the mechanical properties of composites with smaller nanoparticles (< 500 nm) due to the dominant effect of the excess polymer phase from the solvation shell, a topic discussed in greater detail later.

In the case of the micron-sized platelets in the MMA-HEMA mixture, the surface modification with MMA-propyl-, aminopropyl-silanes, and vitrimers showed a similar trend — a better packing density for an MMA-stabilized colloid (31% vs 28%) (Fig. 3 d). However, the differences in the packing density are less pronounced in these systems, indicating that the nature of colloidal interactions between large micron-sized particles was not the decisive parameter in the assembly.

The second aspect of colloidal stabilization — a particle concentration — means that diluted suspensions generally yield better colloidal crystals due to the suppression of multiple nucleation and fast uncontrolled growth, although it always comes at the cost of scalability. In the art of colloidal crystal preparation, typical concentrations of nanoparticles rarely exceed 2–5 vol.%, and this value can become even lower for particles with a high aspect ratio. Studies on cellulose-clay thin films with exceptional mechanical properties showed that reducing the colloid concentration from a dilute 1.6 wt% to an extra-dilute 0.1 wt% was necessary to achieve a significant improvement in particle packing density [46, 47]. In our colloids, reducing the concentration of platelets from typical 20 to 5 vol.% did not show significant improvements, suggesting that not the reduced concentration of the initial stocks in itself but rather the improved particle mobility and capability to rearrangement are the governing parameters in the assembly of platelets into a densely packed structure.

In other words, appropriate surface treatment is a key factor in ensuring colloidal stability during self-assembly and, consequently, achieving the densest possible particle packing. While colloidal interactions play a critical role in systems with small particles (< 500 nm), their significance diminishes in suspensions of heavier micron-sized particles, where other factors — such as gravitational forces and particle inertia — become more dominant.

The effects of anisotropy and particle size distribution The aspect ratio of the particles has a huge impact on the packing probability due to the added degree of freedom related to platelet orientation. The inherently impaired ability of high-aspect-ratio particles to densely pack has been well-documented, particularly in studies on the viscosities of particle suspensions [49], where the effect becomes more pronounced at higher concentrations. This fundamental property of anisotropic particles puts a limitation on suspension concentrations used for self-assembly and poses practical challenges in composite fabrication. Once stacking defects occur, and more effort is required to reorganize misaligned platelets compared to spherical particles. To mitigate these defects, we pre-assembled a colloid of 15 vol.% MMA-modified alumina platelets in HEMA monomer under milder conditions — using gravitational forces and agitation in a shaker for several hours — allowing some degree of particle rearrangement. This approach led to a composite with a higher ceramic loading (35% vs. 29% in the composite without pre-assembly) and an improved elastic modulus (14.5 GPa vs. ~ 11 GPa for the non-pre-assembled sample, Fig. SI7). However, further techniques involving controlled agitation and liquid flow could potentially enhance particle packing density even more.

Another possible solution to overcoming this problem of insufficient packing density is the use of polymodal particle mixtures with lower aspect ratios, where the particle size distribution is tuned to maximize particle packing. The approach was reported to further reduce the viscosity of the stock suspensions [50–52], which is an extremely important parameter in the preparation of composite materials with the highest ceramic loading. Our results also confirm that polydisperse low-aspect-ratio particles can achieve comparable values of stiffness with minimum efforts on particle compaction (Figs. 4 a and 5 b).

4.2 Plastic deformation and fracture behavior in the composites

The effect of the polymer confinement on ductility While the strength and elastic modulus of the composites with different ceramic constituents varied in a relatively narrow range ($\sigma \sim$ 80–150 MPa, $E \sim$ 10–25 MPa), the fracture behavior showed more significant differences across the samples. For the same ceramic volume fraction of 35–55%, the composites with small 80–450-nm spheres always failed as a brittle material despite having a lower effective elastic modulus, while the stiffer samples with large platelets and irregular nanoparticles showed some softening at high strains. This softening was only observed for the composites with non-cross-linked polymers like PHEMA and PMMA (Fig. 3 a), indicating that plastic deformation of the ductile polymer chains was the main reason behind this phenomenon.

Why did composites with the small spheres always break in a brittle manner despite having the same type and amount of polymer as the composites with the larger particles? As previously mentioned, the ability of smaller nanoparticles to "stiffen" dispersed systems more effectively has been extensively reported and explained in terms of the increased

specific surface area (SSA) [45, 53]. However, simple estimations for the same volume fraction of 300-nm spheres and 0.15 × 10-µm platelets gave an almost identical SSA value of ~ 15–20 m^2/cm^3, and yet the bars of these composites showed very different plasticity at high strains (see SI. "9. Estimation of the SSA"). This suggests that other effects define the material deformation behavior.

In an ideal densely packed assembly, the characteristic size of polymer-filled voids strongly depends on the size of particles comprising the structure (D_{voids} ~ 0.23–0.41D_{sphere} in hcp, for example). From a physicochemical perspective, the properties of polymer chains in nanoconfinement can differ significantly from those in bulk, with changes in glass transition temperatures not only at the interface but extending up to hundreds of nanometers into the material [54]. In this context, we propose shifting the focus from particle surface area to the characteristic size of the polymer regions. Composite ductility should be evaluated based on the fraction of different polymer types: (1) chains with limited mobility, confined by the particle surface [38, 53], and (2) chains in quasi-bulk regions that retain the ductility of the pure bulk polymer.

Assuming a constant polymer volume fraction of 0.45 and a rather modest thickness of the affected confined polymer layer of ~ 10 nm, we already obtain ~ 90% of the polymer in a confined state for 100-nm spheres, ~ 25% for 300-nm spheres and ~ 15% for micron-sized platelets (see SI "Estimation of the polymer confinement," Fig. 6 a). Since the confinement effects can easily span over distances 200–300 nm according to a recent review [54], all of the polymer phase in the composites with 80–450 nm spheres is expected to be "stiffer," which was experimentally observed in our study. The assembly of micron-sized particles, on the other hand, provides ample opportunities for the formation of micron-sized polymer regions that are less affected by the confinement effect. In line with this nanoconfinement hypothesis, we observed the highest ductility at high strains for the composites containing the largest 1 × 75-µm platelets with the highest aspect ratio (Fig. 6 b).

Fracture behavior and energy absorption A more detailed analysis of the stress–strain curves for the notched samples revealed an expected trend: the composites with small silica spheres showed an unstable crack propagation (not shown on the graphs), while the samples with larger and more anisotropic particles had a fracture behavior characteristic of nacre including crack deflection as seen in Fig. 7a–f. The toughness of the composites, calculated from the total area under the load–displacement curve and normalized to the final crack cross-section, was also shown to increase with the particle aspect ratio (Table 2).

On the one hand, anisotropic particles increase the effective crack propagation path, thereby facilitating the energy absorption capacity of the material. On the other hand, in light of our findings on the polymer ductility in nanoconfinement, the assembly of high-aspect-ratio particles is also associated with larger and more ductile polymer domains due to the stacking defects, which increases stress dissipation via plastic deformation (observed in the stress–strain curves) and also contributes to the toughness. Decoupling between these phenomena is not trivial and could be an interesting challenge for the theoretical modeling, which is, however, outside of the scope of our manuscript.

Despite the dominant role of polymer plastic deformation in the composite's overall mechanical response, the influence of particle surface treatment on mechanical and fracture behavior remained noticeable for the micron-sized

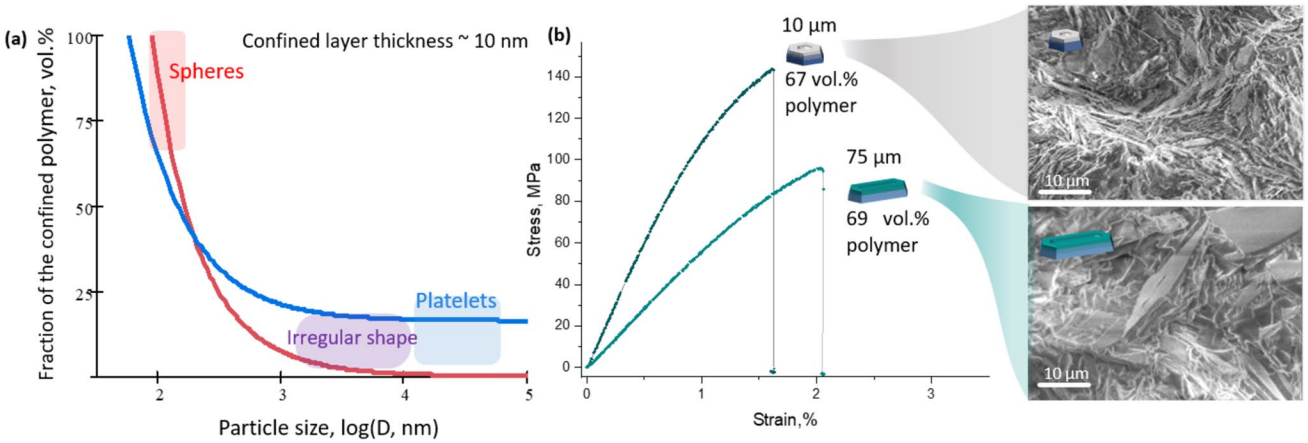

Fig. 6 **a** The estimation of the polymer fraction confined within 10 nm from the particle surface for various ceramic fillers, with the highlighted regions representing the range of the studied samples; **b** stress–strain curves for the composites loaded with platelets, illustrating the improved ductility at high strains for a higher aspect ratio despite small differences in the total polymer content

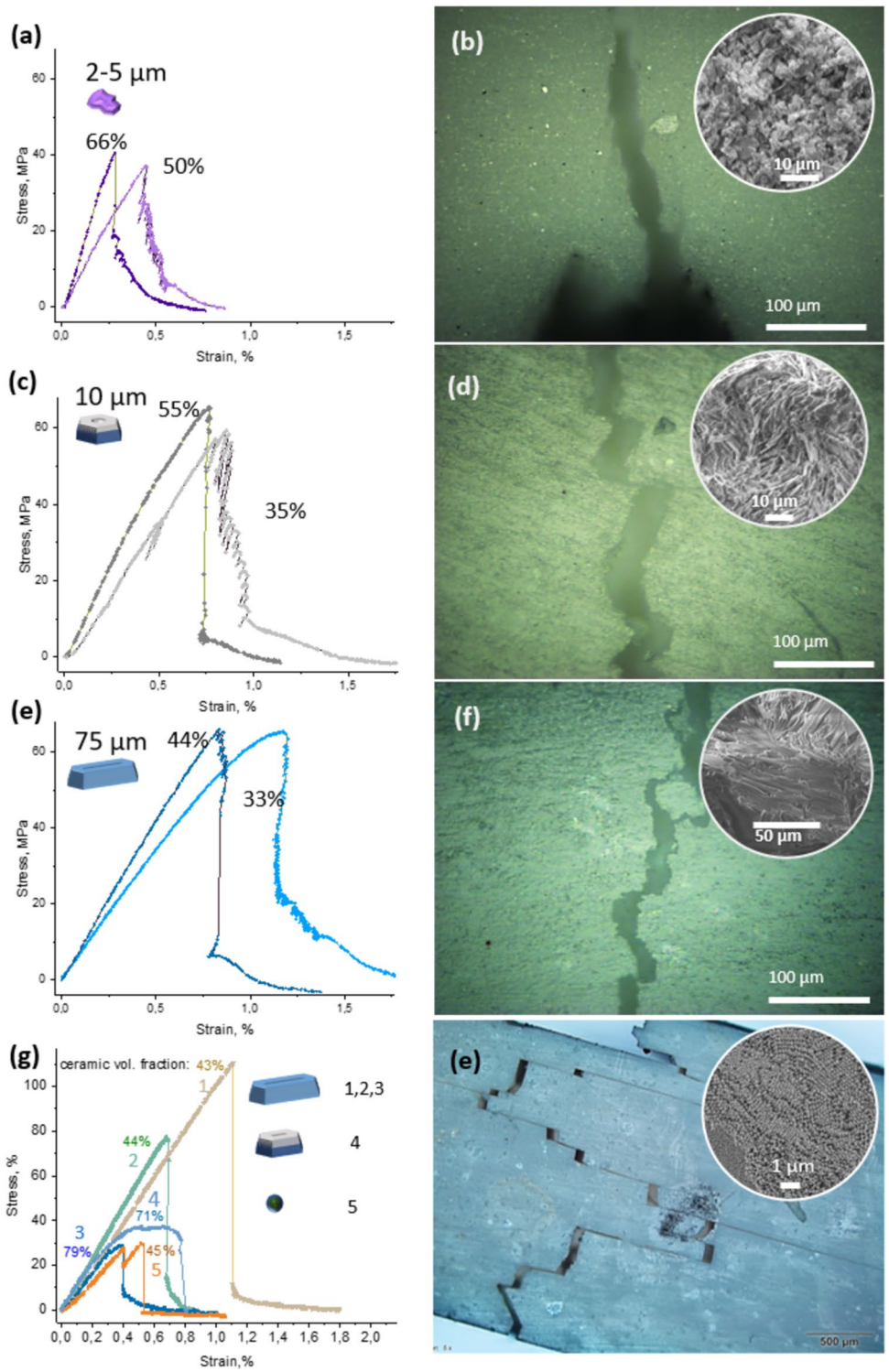

Fig. 7 Stress–strain curves of the notched composites with the corresponding optical images of the propagated crack: **a**, **b** 2–5-µm irregularly shaped particles, **c**, **d** 0.1 × 10-µm platelets, **e**, **f** 1 × 75-µm platelets in the PHEMA matrix. The volume fraction of ceramic loading estimated by TGA is added in % for each composite

platelets (smaller spherical particles were excluded from the analysis due to the stronger impact of surface treatment on packing density). Untreated oxide particles showed earlier crack formation and lower mechanical strength, likely due to weaker bonding between the polymer and the oxide surface (Fig. 3c,d). The difference between MMA- and aminopropyl-treated particles was less significant, with MMA-modified fillers exhibiting a slightly earlier onset of crack propagation, possibly related to the improved bonding (Fig. 3 d). However, the resistance of the polymer phase to crack propagation seems to be the key factor in the fracture behavior of the studied composite materials since the

Table 2 Fracture properties of the notched composites featuring stable crack propagation

Material	Org. volume fraction by TGA, %	Total toughness[a], J/m^2	Toughness after the fracture onset[b], J/m^2	Share of stress–strain area after the fracture onset[b], %
PHEMA polymer	100	75	4	5
2–5-µm irregularly shaped alumina particles in PHEMA	34	53	12	22
	50	54	16	29
0.1 × 10-µm alumina platelets in PHEMA	45	225	18	8
	65	328	82	25
0.1 × 75-µm silica platelets in PHEMA	56	252	28	11
	67	324	42	13

[a]Calculated from the total area under the load–displacement curve

[b]Calculated from the fraction of the area under the load–displacement curve corresponding to fracturing

variations in polymer stiffness (e.g., Styrene, TEGDMA crosslinks) showed a more pronounced effect on the stress–strain behavior (Fig. 3 a).

5 Conclusions

The development of nacre-like ceramic-based materials with exceptional toughness has been a significant challenge for decades due to the difficulty in achieving dense packing of ceramic building blocks on a macroscopic scale, especially for high-aspect-ratio particles. Most successful efforts are typically confined to assembling ceramic particles in thin films or micro-scale structures (e.g., via ice-templating), with repeated cycles required to create larger samples. However, producing thicker samples in a single batch often fails to replicate the same mechanical benefits.

In this study, we explored a more practical approach to fabricating "non-ideal" bio-inspired materials using concentrated colloids (30–50 vol.% for spheres and 15–20 vol.% for platelets) to investigate whether mimicking nacre design in non-densely packed composites can still deliver exceptional mechanical performance compared to the conventional ceramic-in-polymer composites with a wide particle size distribution. Centimeter-scale bulk composites were prepared by a direct assembly from concentrated colloidal suspensions through sedimentation, centrifugation, and/or hot pressing, followed by polymerization. Silica and alumina spheres (80–450 nm) and platelets (0.15 × 10 µm and 1 × 75 µm) were used as the ceramic phase, while various polymers like PHEMA, PMMA, and other functionalized derivatives formed the soft phase. In a single-batch process and without directing forces, the composites achieved a ceramic loading of 55–65%, a flexural strength of 100–150 MPa, and a flexural modulus of 10–25 GPa. High-aspect-ratio ceramic fillers significantly improved the total material's toughness due to the both increased crack propagation path and facilitated plastic deformation of polymer in the large interparticle voids.

The hierarchical structure, size, and shape of the ceramic blocks did not have the expected significant effects on the material strength and stiffness when the ceramic loading was less than 65 vol.%. Larger ceramic blocks with higher aspect ratios generally enhanced the composite stiffness more effectively than spherical particles, as predicted by theoretical models. However, this benefit was significantly limited in practice due to the reduced packing density of the highly anisotropic platelets.

In summary, the results emphasize the superior role of particle packing over other factors such as particle anisotropy or hierarchy. Several strategies were suggested to enhance packing density: reducing the particle aspect ratio to facilitate rearrangement, using an optimized polymodal particle size distribution, and maximizing colloidal stabilization in the suspensions by aligning the particle surface chemistry with the monomer properties. Another key limitation on packing density stems from the absolute particle size, particularly for smaller particles (< 300 nm). In these cases, solvation shells significantly contribute to the total organic content, capping the maximum ceramic loading. As a result, composites with 80–450-nm spheres, despite achieving near-theoretical packing densities, could not surpass an elastic modulus of ~ 10 GPa in this study. This phenomenon is expected to apply to all small colloidal nanoparticles with high surface-to-volume ratios, regardless of aspect ratio.

Mechanical failure predominantly occurred within the polymer phase, meaning the amount of the soft phase, and its plasticity had a greater influence on the mechanical properties than the type of interface bonding. Notably, at a similar polymer volume fraction, composites with small spherical particles (< 500 nm) always exhibited brittle failure, whereas those loaded with platelets displayed ductile behavior under high strains. This behavior can be explained by the different chain mobility of polymers in small and large intraparticle voids, supported by recent theoretical

and experimental studies on the effects of spatial confinement on polymer properties. According to this hypothesis, polymers confined between smaller particles may exhibit a "stiffer" mechanical response, an effect that should be factored into both theoretical modeling and experimental design of composites.

Based on our findings, future research on ceramic-in-polymer composite materials should be focused on achieving the exceptional packing density of the building blocks using the latest developments in colloidal self-assembly and top-down manufacturing. From a practical point of view, however, a significant improvement of the mechanical strength, stiffness, and toughness of the ceramic-in-polymer composites can be achieved by a simple optimization of the particle size distribution without utilizing highly anisotropic particles or complex hierarchical designs.

Supplementary Information The online version contains supplementary material available at https://doi.org/10.1007/s42114-024-01107-x.

Acknowledgements The authors would like to thank Dr. Philipp Haida for kindly providing vitrimer blocks used for surface modifications of some ceramic fillers.

Author contribution V.Semeykina participated in conceptualization, did experimental work, and wrote the main manuscript text. C.Appiah and S.Rothberg did experiments and analyzed the data. S.Heinrich provided project supervision, D.Giuntini and G. Schneider provided supervision, research conceptualization and data analysis. All authors reviewed the manuscript.

Funding Open Access funding enabled and organized by Projekt DEAL. This work was funded by the German Research Foundation (Deutsche Forschungsgemeinschaft, DFG), project number 192346071, SFB 986 "Tailor-Made Multi-Scale Materials Systems."

Data availability No datasets were generated or analysed during the current study.

Declarations

Declaration of generative AI in scientific writing No generative AI was used in the preparation of the present manuscript.

Competing interests The authors declare no competing interests.

References

1. Pan H, She W, Zuo W et al (2020) Hierarchical toughening of a biomimetic bulk cement composite. ACS Appl Mater Interfaces 12:53297–53309
2. Zandinejad AA, Atai M, Pahlevan A (2006) The effect of ceramic and porous fillers on the mechanical properties of experimental dental composites. Dent Mater 22:382–387
3. Marin E (2023) History of dental biomaterials: biocompatibility, durability and still open challenges. Herit Sci 11:207
4. Porto T, Roperto R, Porto-Neto S et al (2017) Polymer-infiltrated-ceramic-network the evolution of CAD/CAM materials. EC Dent Sci 13:94–98
5. Meyers MA, Chen PY, Lin AYM et al (2008) Biological materials: structure and mechanical properties. Prog Mater Sci 53:1–206
6. Sun J, Bhushan B (2012) Hierarchical structure and mechanical properties of nacre: a review. RSC Adv 2:7617–7632
7. Bouville F, Maire E, Meille S et al (2014) Strong, tough and stiff bioinspired ceramics from brittle constituents. Nat Mater 13:508–514
8. Morits M, Verho T, Sorvari J et al (2017) Toughness and fracture properties in nacre-mimetic clay/polymer nanocomposites. Adv Funct Mater 27:1605378
9. Maghsoudi-Ganje M, Lin L, Wang X et al (2019) Bioinspired design of hybrid composite materials. Int J Smart Nano Mater 10:90–105
10. Song J, Chen C, Zhu S et al (2018) Processing bulk natural wood into a high-performance structural material. Nature 554:224–228
11. Özduman ZC, Oglakci B, Halacoglu Bagis DM, Aydogan Temel B, Eliguzeloglu Dalkilic E (2023) Comparison of a nanofiber-reinforced composite with different types of composite resins. Polymers (Basel) 15:3628
12. An Y, Han J, Zhang X et al (2016) Bioinspired high toughness graphene/ZrB2 hybrid composites with hierarchical architectures spanning several length scales. Carbon N Y 107:209–216
13. Jiao D, Qu RT, Weng ZY et al (2019) On the fracture mechanisms of nacre: effects of structural orientation. J Biomech 96:109336
14. Li XW, Ji HM, Yang W et al (2017) Mechanical properties of crossed-lamellar structures in biological shells: a review. J Mech Behav Biomed Mater 74:54–71
15. Yang X-Y, Chen L-H, Li Y et al (2017) Hierarchically porous materials: synthesis strategies and structure design. Chem Soc Rev 46:481–558
16. Barthelat F, Tang H, Zavattieri PD et al (2007) On the mechanics of mother-of-pearl: a key feature in the material hierarchical structure. J Mech Phys Solids 55:306–337
17. Li H, Xu Z-H, Li X (2013) Multiscale hierarchical assembly strategy and mechanical prowess in conch shells (Busycon carica). J Struct Biol 184:409–416
18. Lin AY-M, Chen P-Y, Meyers MA (2008) The growth of nacre in the abalone shell. Acta Biomater 4:131–138
19. Studart AR (2016) Additive manufacturing of biologically-inspired materials. Chem Soc Rev 45:359–376
20. Wegst UGK, Bai H, Saiz E et al (2015) Bioinspired structural materials. Nat Mater 14:23–36
21. Peng J, Cheng Q (2017) High-performance nanocomposites inspired by nature. Adv Mater 29:1702959
22. Le Ferrand H, Bouville F, Niebel TP et al (2015) Magnetically assisted slip casting of bioinspired heterogeneous composites. Nat Mater 14:1172–1179
23. Mirabello G, Ianiro A, Bomans P et al (2020) Crystallization by particle attachment is a colloidal assembly process. Nat Mater 4:391–396

24. Bonderer LJ, Studart AR, Gauckler LJ (2008) Bioinspired design and assembly of platelet reinforced polymer films. Science (80-) 319:1069–1073
25. Podsiadlo P, Kaushik AK, Arruda EM et al (2007) Ultrastrong and stiff layered polymer nanocomposites. Science (80-) 318:80–83
26. Dreyer A, Feld A, Kornowski A et al (2016) Organically linked iron oxide nanoparticle supercrystals with exceptional isotropic mechanical properties. Nat Mater 15:522–528
27. Georgopanos P, Schneider GA, Dreyer A, Handge UA et al (2017) Exceptionally strong, stiff and hard hybrid material based on an elastomer and isotropically shaped ceramic nanoparticles. Sci Rep 7:7314
28. Munch E, Launey ME, Alsem DH et al (2008) Tough, bio-inspired hybrid materials. Science (80-) 322:1516–1520
29. Lassila L, Keulemans F, Vallittu PK et al (2020) Characterization of restorative short-fiber reinforced dental composites. Dent Mater 39:992–999
30. Launey ME, Munch E, Alsem DH et al (2009) Designing highly toughened hybrid composites through nature-inspired hierarchical complexity. Acta Mater 57:2919–2932
31. Bu Y, Wang X, Bu X et al (2023) Self-assembling nacre-like high-strength and extremely tough polymer composites with new toughening mechanism. J Mater Sci Technol 136:236–244
32. Cui B-C, Li J, Lin Y-H et al (2019) Polymer-infiltrated layered silicates for dental restorative materials. Rare Met 38:1003–1014
33. Ikeda H, Kawajiri Y, Sodeyama MK et al (2022) A SiO2/pHEMA-based polymer-infiltrated ceramic network composite for dental restorative materials. J Compos Sci 6:17
34. Skorulska APP, Rybak Z, Szymonowicz M et al (2021) Review on polymer, ceramic and composite materials for CAD/CAM indirect restorations in dentistry-application: mechanical characteristics and comparison. Materials (Basel) 14:1592
35. Jelitto H, Felten F, Swain MV et al (2007) Measurement of the total energy release rate for cracks in PZT under combined mechanical and electrical loading. J Appl Mech 74:1197–1211
36. Zhao H, Zhao Y, Lin G (2018) Nacre-inspired composites with different macroscopic dimensions: strategies for improved mechanical performance and applications. NPG Asia Mater 10:1–22
37. Abuelenain DA, Neel EAA, Al-Dharrab A (2015) Surface and mechanical properties of different dental composites. Austin J Dent 2:1019
38. Rajinthan L, Fritz S, Galkov I et al (2023) Nacre-like composites with a soft thermoplastic elastomer matrix. Compos Sci Technol 244:110302. https://doi.org/10.1016/j.compscitech.2023.110302
39. Tushtev K, Murck M, Grathwohl G (2008) On the nature of the stiffness of nacre. Mater Sci Eng C 28:1164–1172
40. Kroner E (1958) Berechnung der elastischen Konstanten des Vielkristalls aus des Konstanten des Einkristalls. Z Phys 151:504–518
41. Jäger I, Fratzl P (2000) Mineralized collagen fibrils: a mechanical model with a staggered arrangement of mineral particles. Biophys J 79(4):1737–1746. https://doi.org/10.1016/S0006-3495(00)76426-5
42. Begley MR, Philips NR, Compton BG et al (2012) Micromechanical models to guide the development of synthetic "brick and mortar" composites. J Mech Phys Solids 60:1545–1560
43. Stempflé P, Pantalé O, Rousseau M et al (2010) Mechanical properties of the elemental nanocomponents of nacre structure. Mater Sci Eng C 30:715–721
44. Greco F, Leonetti L, Pranno A et al (2020) Mechanical behavior of bio-inspired nacre-like composites: a hybrid multiscale modeling approach. Compos Struct 233:111625. https://doi.org/10.1016/j.compstruct.2019.111625
45. Fu SY, Feng XQ, Lauke B et al (2008) Effects of particle size, particle/matrix interface adhesion and particle loading on mechanical properties of particulate-polymer composites. Compos Part B Eng 39:933–961
46. Li L, Maddalena L, Nishiyama Y et al (2022) Recyclable nanocomposites of well-dispersed 2D layered silicates in cellulose nanofibril (CNF) matrix. Carbohydr Polym 279:119004. https://doi.org/10.1016/j.carbpol.2021.119004
47. Liu A, Walther A, Ikkala O et al (2011) Clay nanopaper with tough cellulose nanofiber matrix for fire retardancy and gas barrier functions. Biomacromol 12:633–641
48. Polte J (2015) Fundamental growth principles of colloidal metal nanoparticles - a new perspective. CrystEngComm 17:6809–6830. https://doi.org/10.1039/C5CE01014D
49. Mueller S, Llewellin EW, Mader HM (2010) The rheology of suspensions of solid particles. Proc R Soc A 466:1201–1228
50. Greenwood R, Luckham PF, Gregory T (1998) Minimising the viscosity of concentrated dispersions by using bimodal particle size distributions. Colloids Surfaces A Physicochem Eng Asp 144:139–147
51. Zaman AA, Dutcher CS (2006) Viscosity of electrostatically stabilized dispersions of monodispersed, bimodal, and trimodal silica particles. J Am Ceram Soc 89:422–430
52. Pal R (2023) Recent progress in the viscosity modeling of concentrated suspensions of unimodal hard spheres. ChemEngineering 7:70
53. Jiang Y, Tohgo K, Yang H (2010) Study of the effect of particle size on the effective modulus of polymeric composites on the basis of the molecular chain network microstructure. Comput Mater Sci 49:439–443. https://doi.org/10.1016/j.commatsci.2010.05.015
54. Roth CB (2021) Polymers under nanoconfinement: where are we now in understanding local property changes? Chem Soc Rev 50:8050–8066